Palm-Print Classification by Global Features

Bob Zhang, *Member, IEEE*, Wei Li, Pei Qing, and David Zhang, *Fellow, IEEE*

***Abstract*—Three-dimensional (3-D) palm print has proved to be a significant biometrics for personal authentication. Three-dimensional palm prints are harder to counterfeit than 2-D palm prints and more robust to variations in illumination and serious scrabbling on the palm surface. Previous work on 3-D palm-print recognition has concentrated on local features such as texture and lines. In this paper, we propose three novel global features of 3-D palm prints which describe shape information and can be used for coarse matching and indexing to improve the efficiency of palm-print recognition, particularly in very large databases. The three proposed shape features are maximum depth of palm center, horizontal cross-sectional area of different levels, and radial line length from the centroid to the boundary of 3-D palm-print horizontal cross section of different levels. We treat these features as a column vector and use orthogonal linear discriminant analysis to reduce their dimensionality. We then adopt two schemes: 1) coarse-level matching and 2) ranking support vector machine to improve the efficiency of palm-print recognition. We conducted a series of 3-D palm-print recognition experiments using an established 3-D palm-print database, and the results demonstrate that the proposed method can greatly reduce penetration rates.**

***Index Terms*—Global features, orthogonal linear discriminant analysis (LDA) (OLDA), palm-print indexing, ranking support vector machine (SVM) (RSVM), 3-D palm-print identification.**

I. Introduction

PALM-PRINT recognition has now been a topic of research for over 10 years. Like other biometrics, palm prints demonstrate the properties required for personal authentication: universality, uniqueness, permanence, collectability, and acceptability [1]. Furthermore, palm prints have some advantages over other biometrics. Palm prints are larger than fingerprints and therefore more robust to scars and dirt. Palm-print images are cheaper to collect and more acceptable than iris. Palm prints can distinguish between individuals more accurately than face and can also identify monozygotic twins [2].

Manuscript received March 21, 2011; revised August 5, 2011 and February 13, 2012; accepted April 14, 2012. Date of publication January 28, 2013; date of current version February 12, 2013. This work was supported in part by the General Research Fund from the Hong Kong Special Administrative Region Government, by the central fund from The Hong Kong Polytechnic University, and by the National Natural Science Foundation of China Oversea fund (61020106004), China. This paper was recommended by Associate Editor J. Wu.

B. Zhang is with the Biometrics Research Center, Department of Computing, The Hong Kong Polytechnic University, Kowloon, Hong Kong, and also with the Department of Electrical and Computer Engineering, University of Waterloo, Waterloo, ON N2L 3G1, Canada (e-mail: yibo@pami.uwaterloo.ca).

W. Li is with the Shenzhen Institutes of Advanced Technology, Chinese Academy of Sciences, Shenzhen 518055, China, and also with Huawei Technologies Company, Ltd., Shenzhen 518129, China (e-mail: liweistorm@126.com).

P. Qing and D. Zhang are with the Biometrics Research Center, Department of Computing, The Hong Kong Polytechnic University, Kowloon, Hong Kong (e-mail: edwardtoday@gmail.com; csdzhang@comp.polyu.edu.hk).

Color versions of one or more of the figures in this paper are available online at http://ieeexplore.ieee.org.

Digital Object Identifier 10.1109/TSMCA.2012.2201465

Traditionally, palm-print recognition has made use of either high- or low-resolution 2-D palm-print images. High-resolution images are suitable for forensic applications [3], while low-resolution images are suitable for civil and commercial applications [4]. Most current research uses low-resolution palm-print recognition and is either texture based or line based. The texture-based methods include PalmCode [4], Competitive Code [5], and Ordinal Code [6]. These methods use a group of filters to enhance and extract the phase or directional features which can represent the texture of the palm print. Line-based methods use line or edge detectors to explicitly extract line information from the palm print that is then used for matching. The representative methods include derivative-of-Gaussian-based line extraction [7] and modified-finite-Radon-transform-based line extraction [8].

In recent years, 3-D techniques have been applied to biometric authentication, such as 3-D face [9], [10] and 3-D ear recognition [11]. Most recently, a structured-light-imaging [12], [13] 3-D palm-print system [14], [15] was developed that captures the depth information of a palm print. This information is then used to calculate the mean and the Gaussian curvatures for use in 3-D palm-print matching and recognition. To date, however, there has been no work with 3-D palm prints that has extracted global shape features, which may be useful in classification and indexing. For fingerprint, according to the global ridge structure and singularities, it can be classified into five classes: arch, tented arch, left loop, right loop, and whorl [16]. Reference [17] classified the palm print into six classes according to the palm-print principal lines. Besides the exclusive classification technique, the continuous classification technique is also widely used for indexing the database for personal identification [18].

In this paper, we propose extracting three novel global features from a 3-D palm-print image: maximum depth (MD) at the center of the palm, horizontal cross-sectional area (HCA) at different levels of the palm; and radial line length (RLL) measured from the centroid to the boundary of the 3-D palm print. These features are then used to describe and classify the shape of the 3-D palm print using continuous classification. This involves first reducing the dimensionality of the features by treating these features as a column vector and applying orthogonal linear discriminant analysis (LDA) (OLDA) [19]. We then improve the efficiency of palm-print recognition by indexing the database using coarse-level matching and ranking support vector machine (SVM) (RSVM) [20].

The rest of this paper is organized as follows. Section II describes how we define a region of interest (ROI) for the 3-D palm-print image and then extract our three proposed global features. Section III describes how global features can be used in classification in order to speed up identification. Section IV gives the experimental results, and Section V concludes this paper.

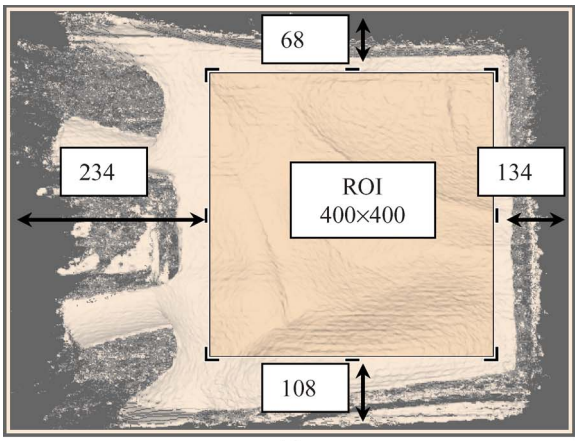

(a)

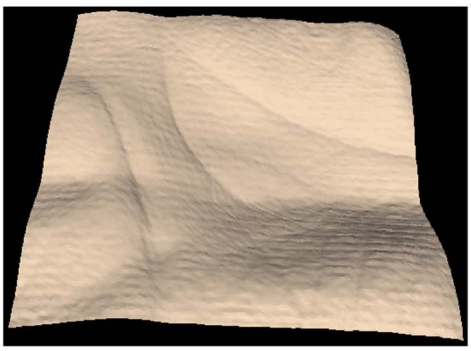

(b)

Fig. 1. ROI extraction of 3-D palm print. (a) Location of the ROI in the 3-D palm-print image. (b) Extracted 3-D ROI.

II. Global Features: Definitions and Extraction

The following describes our procedure by first extracting a region of interest from the 3D palmprint, and from each palmprint extract our proposed three global features.

A. ROI

Our definition and extraction procedure makes use of a 3-D palm-print image containing 768 × 576 points captured using a structured-light-imaging-based 3-D palm-print acquisition device [14]. First, we remove redundant and noisy boundary regions using a very simple ROI extraction process (Fig. 1). We segment a 400 × 400 point square that is 68, 108, 234, and 134 points from the top, bottom, left, and right boundaries of the 3-D palm-print image, respectively, as shown in Fig. 1(a). Fig. 1(b) shows the extracted ROI. After downsampling the 3-D ROI to 200 × 200 points, we store it in a 200 by 200 matrix, $\{d_{ij}|i = 1, 2, \ldots, 200; j = 1, 2, \ldots, 200\}$, where d_{ij} is the depth value of the ith row and jth column point of the 3-D ROI.

Our proposed 3-D palm-print ROI extraction approach is much simpler than the one reported in [4], and the extracted shape features are not sensitive to translation and rotation, which is why we can use such a coarse ROI extraction. As the shape feature is a form of global feature, we extract as large a ROI as possible. Of course, such a large ROI may contain noisy data, so we use a mask to remove the noisy data according to

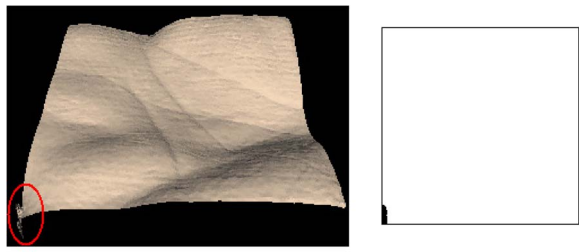

(a) (b)

Fig. 2. (a) Three-dimensional ROI with noise. (b) Mask of the 3-D ROI.

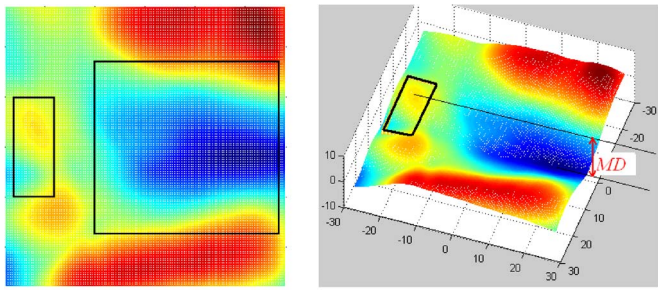

(a) (b)

Fig. 3. Illustration of the MD feature (with color denoting the depth of the 3-D ROI). (a) Location of the two rectangles used to calculate the reference plane and to find the MD point. (b) Illustration of the MD feature.

the gradient of the 3-D data. If the gradient of the point, which is defined as $|\nabla d| = \sqrt{(\partial d/\partial x)^2 + (\partial d/\partial y)^2}$, is larger than a given threshold, the point is regarded as noisy data. Fig. 2 shows a 3-D ROI which contains noisy data and its corresponding mask. We use a 200 by 200 matrix, $\{m_{ij}|i = 1, 2, \ldots, 200; j = 1, 2, \ldots, 200\}$, to represent the mask, where $m_{ij} = 0$ is noisy data and $m_{ij} = 1$ is for other data.

B. Three Global Features

Using the ROI obtained from the original 3-D palm-print data, we extract three kinds of features to describe the shape of the 3-D palm print: MD of palm center, the HCA of different levels, and the RLL from the centroid to the boundary of 3-D palm-print horizontal cross section of different levels.

1) MD: MD means the maximum depth value of the 3-D palm from a reference plane. The reference plane is decided using a rectangle as shown in the left of Fig. 3(a). The depth of the reference plane d_r is the mean depth of the points contained by this rectangle

$$d_r = \frac{1}{\sum_{i=R_s}^{R_e}\sum_{j=C_s}^{C_e} m_{ij}} \sum_{i=R_s}^{R_e}\sum_{j=C_s}^{C_e} (d_{ij} \cdot m_{ij}) \qquad (1)$$

where d_{ij} is the depth value of the ith row and jth column point of the 3-D ROI, m_{ij} is the corresponding mask value, and R_s, R_e, C_s, and C_e denote the start row, end row, start column, and end column, respectively. The parameters $R_s = 65$, $R_e = 136$, $C_s = 6$, and $C_e = 35$ were set by experience. The reason we choose this region is that, in the 3-D ROI, it appears to be relatively flat.

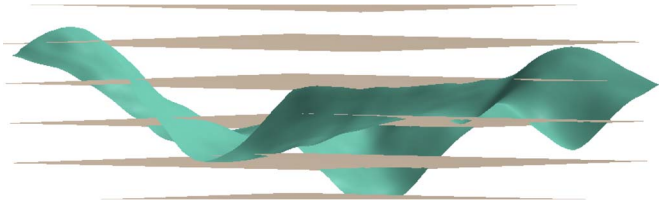

Fig. 4. Illustration of the 3-D ROI crossed by horizontal planes.

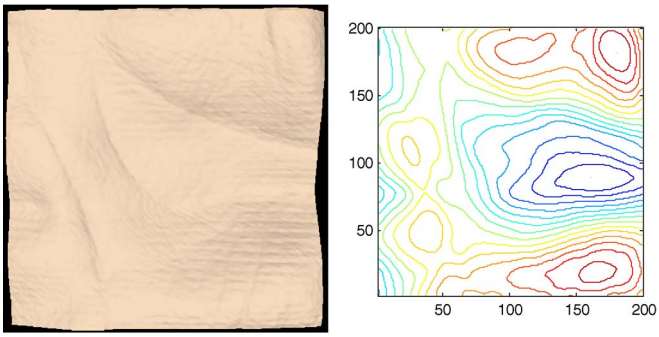

(a) (b)

Fig. 5. (a) Three-dimensional ROI. (b) Its corresponding contour cutting by the equidistant horizontal planes.

After getting the depth of the reference plane, we find the MD $d_{\max}$ in a region denoted by the right rectangle in Fig. 3(a) which starts at the 41st row and extends to the 160th row and from the 65th column to the 190th column. The MD can then be calculated easily by (2) as shown in Fig. 3(b)

$$MD = d_{\max} - d_r. \tag{2}$$

2) HCA: To describe the shape of the 3-D palm print, we use a group of equidistant horizontal planes to cut the 3-D ROI as shown in Fig. 4. Fig. 5 shows a 3-D ROI and its contour cut by the equidistant horizontal planes. To render the shape clearly, Fig. 5(a) only shows the 3-D ROI image and hides the equidistant horizontal planes. In Fig. 5(b), the blue curves denote deeper levels, the red curves denote higher levels, and the remaining curves are medium levels. The HCA is defined as the area enclosed by the level curve. From Fig. 5(b), we can see that most of the deeper level curves are enclosed and the areas are simply connected. These are more stable in response to noise or transformation.

To get a stable HCA, we take into consideration only the levels from the deepest point to the reference plane, defined in Section III-A. Suppose we divide this region into N levels. Every level G^k, $k = 1, 2, \ldots, N$, is described with a 200×200 matrix and calculated by

$$G_{ij}^k = \begin{cases} 1, & \text{if } d_{ij} > h \cdot (N-k+1)/N \\ 0, & \text{otherwise} \end{cases}$$
$$k = 1, 2, \ldots, N;\ i = 1, 2, \ldots, 200;\ j = 1, 2, \ldots, 200 \tag{3}$$

where d_{ij} is the depth value of the ith row and jth column point of the 3-D ROI and h is the palm-print depth defined by (2).

To make it more stable, we constrain every level growing from its previous level except the first level. That is,

$$L^k = G^k \cap (L^{k-1} \oplus \Theta^{k-1}), \quad k = 2, 3, \ldots, N; \quad L^1 = G^1 \tag{4}$$

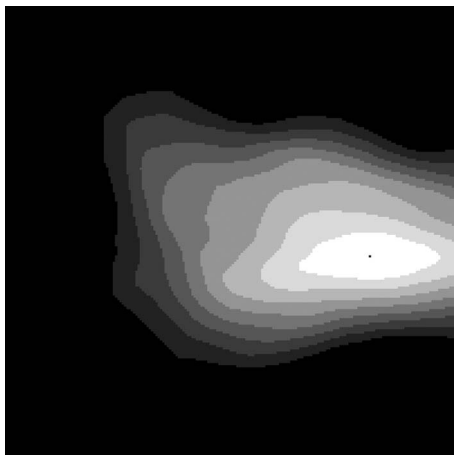

Fig. 6. Example of all the levels stacked together when $N = 8$.

where "$\cap$" denotes logical AND, $\oplus$ denotes a morphological dilation operation, and Θ^k is a disk morphological structuring element whose size can be calculated by $35 - 3 \times k$ (this is suitable for $N = 8$ by experience).

Fig. 6 shows an example of all the levels stacked together. Fig. 7 shows each of the levels separately.

After getting the cross-sectional levels L^k, $k = 1, 2, \ldots, N$, the HCA A^k, $k = 1, 2, \ldots, N$, can be easily calculated by

$$A^k = \sum_{i=1}^{200} \sum_{j=1}^{200} L_{ij}^k. \tag{5}$$

3) RLL: The HCA is only a coarse description of the cross section. To identify samples which have a similar cross-sectional area but a different contour, we propose the RLL feature which describes the shape of the contour. First, we calculate the centroid of the first level L^1; thereafter, we treat it as the centroid of all levels. Then, from the centroid, we draw M radial lines which intersect with the contour of every level. The distance between the intersection and the centroid is defined as the RLL. The radial lines are distributed at equal angles. We record these radial lines from the inner layers to the outer layers starting with the horizontal direction by an $M \times N$ dimensional vector R_i, $i = 1, 2, \ldots, M \times N$, where M is the number of radial lines and N is the number of cross sections. Fig. 8 shows some examples of radial lines and their cross sections. We can see that the RLL better represents the contour as the number of radial lines increases.

The aforementioned three global features are mainly determined by the central region of the palm. This region is certainly contained by the ROI described in Section II-A which makes these features insensitive to translation and rotation. Although the RLL feature can be affected by rotation as the contours change smoothly, if the rotation is small, then the variation of the RLL feature will also be small. There are some restricting pegs on the capture device which can guide the user to put his/her hand on the proper place as described in [14]. Furthermore, we assume that the user is cooperative when collecting data as we aim at civil rather than law enforcement applications.

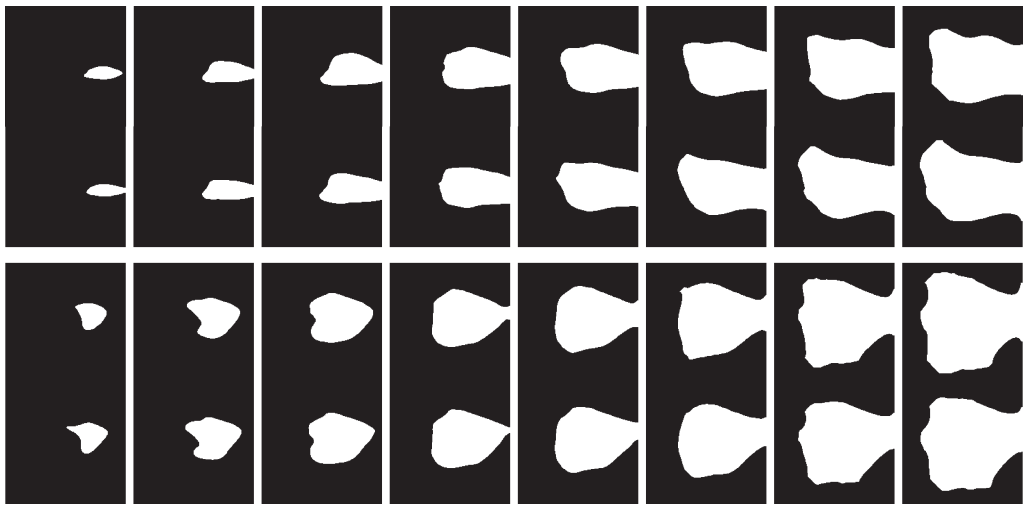

Fig. 7. Cross-sectional area feature (the top two rows are extracted from two samples collected from one palm, and the bottom two rows are extracted from two samples from another palm).

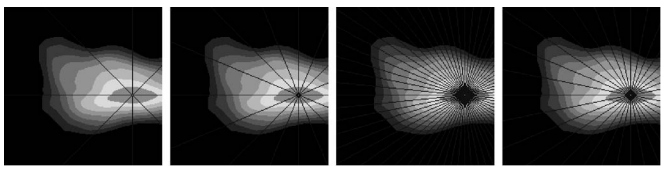

Fig. 8. Radial line starting from the centroid (from left to right: $M = 8,\ 16,\ 32,$ and 64, respectively).

III. Classification With Global Features

The classification of biometrics speeds up the identification process by reducing the number of comparisons that must be made. There are two kinds of classification techniques: exclusive classification and continuous classification. Both fingerprint [16] and palm-print classifications [17] make use of exclusive classification. The main problem of this technique is that it uses only a small number of classes and the samples are unevenly distributed between them, with more than 90% of the samples being in just two or three classes. A further problem with exclusive classification is that, when classification is performed automatically, it is necessary to handle errors and rejected samples gracefully, which is a hard problem in practice. In contrast, for continuous classification, samples are not partitioned into disjoint classes but rather associated with numerical vectors which represent features of the samples. These feature vectors are created through a similarity-preserving transformation so that similar samples are mapped into close points in the multidimensional space [21]. In this paper, we adopt the continuous classification technique. As the global features combining MD, HCA, and RLL are high dimensional, we reduce the dimensions using the LDA method. We then improve the efficiency of palm-print recognition by applying coarse-level matching and RSVM to the low-dimensional vectors.

A. Dimension Reduction Using OLDA

LDA is a state-of-the-art dimensionality reduction technique widely used in classification problems. The objective is to find the optimal projection which simultaneously minimizes the within-class distance and maximizes the between-class distance, thus achieving maximum discrimination (here, the "class" is used to denote the identity of the subjects, e.g., the samples collected from one palm are regarded as one class). However, the traditional LDA requires the within-class scatter matrix to be nonsingular, which means that the sample size should be large enough compared with its dimension, but is not always possible. In this paper, we therefore adopt the OLDA proposed in [19], where the vectors of the optimal projection are calculated using the training database and the optimal projecting vectors are orthogonal to each other.

Suppose that the 3-D ROI has been divided to N levels and that M radial lines are used to represent the level contours. We can list the global features as a column vector, $F=\{MD, A^1, A^2, \ldots, A^N, R^1, R^2, \ldots, R^{N\times M}\}$, with $1+N+N\times M$ rows. Given a training database which has n samples and k classes as $X=[X_1, X_2, \ldots, X_k]$, where $X_i \in \Re^{(1+N+N\times M)\times n_i}$, $i=1,2,\ldots,k$, and $n=\sum_{i=1}^{k} n_i$, adopting OLDA [19], the optimal projection W can be calculated as follows.

First, the within-class scatter matrix S_w, the between-class scatter matrix S_b, and total scatter matrix S_t can be expressed as

$$S_w = H_w H_w^{\mathrm{T}}, \quad S_b = H_b H_b^{\mathrm{T}}, \quad S_t = H_t H_t^{\mathrm{T}} \tag{6}$$

where

$$H_w = \frac{1}{\sqrt{n}}\left[X_1 - m_1 \cdot e_1^{\mathrm{T}}, \ldots, X_k - m_k \cdot e_k^{\mathrm{T}}\right] \tag{7}$$

$$H_b = \frac{1}{\sqrt{n}}\left[\sqrt{n_1}(m_1 - m), \ldots, \sqrt{n_k}(m_k - m)\right] \tag{8}$$

$$H_t = \frac{1}{\sqrt{n}}(X - m \cdot e^{\mathrm{T}}) \tag{9}$$

where m_i is the centroid of the ith class X_i, m is the centroid of all the training samples X, $e_i = [1,1,\ldots,1]^{\mathrm{T}} \in \Re^{n_i}$, $i=1,2,\ldots,k$, and $e=[1,1,\ldots,1]^{\mathrm{T}} \in \Re^{n}$.

After calculating H_w, H_b, and H_t, the reduced singular value decomposition (SVD) is applied to H_t

$$H_t \xrightarrow{\text{Reduced } SVD} U_r \Sigma_r V_r^{\mathrm{T}}. \tag{10}$$

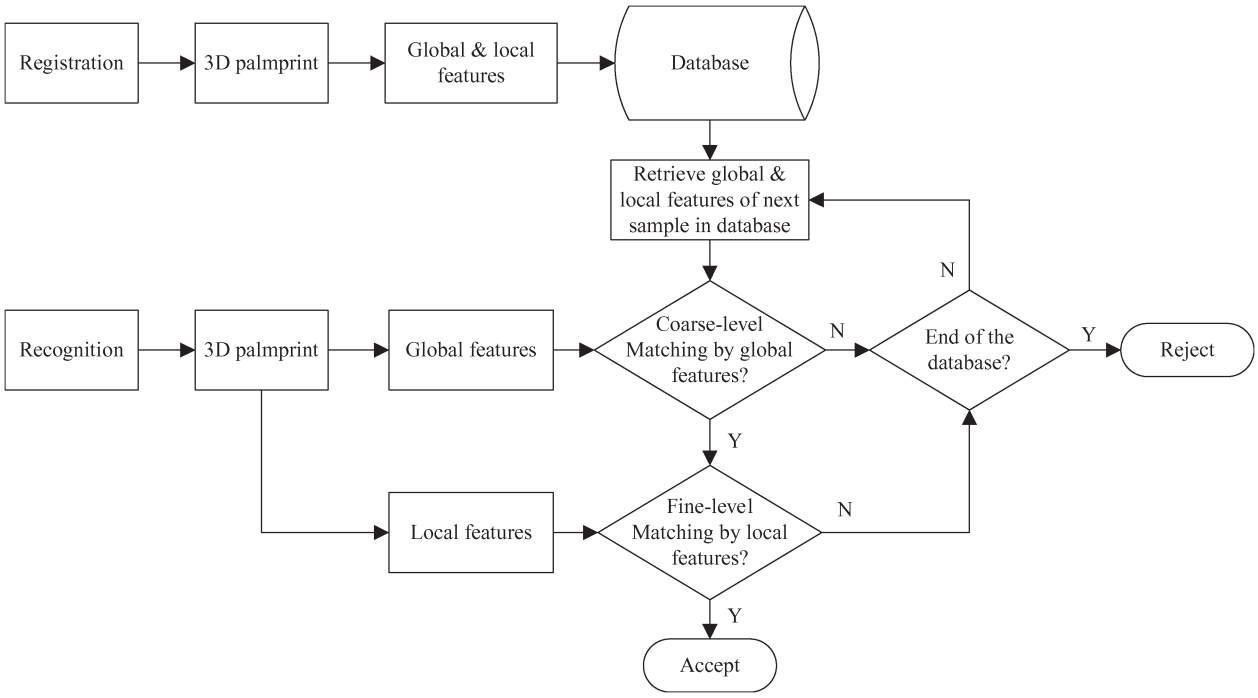

Fig. 9. Flowchart of registration and recognition with coarse-level matching scheme.

Denote $B = \Sigma_r^{-1} U_r^{\mathrm{T}} H_b$, and compute the SVD of B

$$B \xrightarrow{SVD} U_B \Sigma_B V_B^{\mathrm{T}}. \tag{11}$$

Let

$$D = U_r \Sigma_r^{-1} U_B \tag{12}$$

$$q = rank(B) \tag{13}$$

and denote D_q the first q columns of the matrix D. Then, compute the QR decomposition of D_q

$$D_q \xrightarrow{QR \text{ decomposition}} QR \tag{14}$$

where Q is the desired orthogonal matrix and optimal projection, i.e., $W = Q$.

After getting the optimal projection W, we can map the $1+N+N\times M$ dimensional vector F to a lower dimensional space

$$\widetilde{F} = W^{\mathrm{T}} F \tag{15}$$

where $\widetilde{F} = \{f_1, f_2, \ldots, f_\Gamma\}$ is a Γ-dimensional vector with $\Gamma < 1 + N + N \times M$.

B. Coarse-Level Matching

As the purpose of coarse-level matching is to speed up the identification during retrieval, we can regard it as a continuous classification approach. After mapping the global features' Γ-dimensional vector $\widetilde{F}$, the global features can be used to measure the similarity of two samples as follows:

$$\Delta = \|\widetilde{F}^1 - \widetilde{F}^2\|_2 = \sum_{i=1}^{\Gamma} \left(f_i^1 - f_i^2\right)^2. \tag{16}$$

In 3-D palm-print identification, we can use the Γ-dimensional global features to carry out coarse-level matching as shown in Fig. 9. If the testing sample passes coarse-level matching, it undergoes fine-level matching using 3-D palm-print local features. If it does not pass, it moves on to the next sample in the database and so on until it has accessed the last sample in the database. From (16), we can see that coarse-level matching requires only Γ times of addition and multiplication which is much faster than fine-level matching using local features. Equation (17) gives the fine-level matching by mean curvature image (MCI) feature [14]

$$Y = \frac{2\sum_{i=1}^{n}\sum_{j=1}^{m} Z_d(i,j) \cap Z_t(i,j)}{\sum_{i=1}^{n}\sum_{j=1}^{m} Z_d(i,j) + \sum_{i=1}^{n}\sum_{j=1}^{m} Z_t(i,j)} \tag{17}$$

where symbol "$\cap$" represents the logical AND operation and Z_d and Z_t are the two binarized MCI features. To deal with the translation problem of ROI when calculating the matching score by (17), we will shift two, four, six, and eight pixels of the test image along eight directions: right, left, up, down, left–up, left–down, right–up, and right–down, respectively. Adding the nonshift one, we will have $8 \times 4 + 1 = 33$ matching scores, and the maximum one is selected. Suppose the size of the MCI feature is 128×128, i.e., $m = 128$ and $n = 128$, from (16) and (17), we can see that coarse-level matching is much faster than fine-level matching.

C. RSVM

Coarse-level matching scheme is a simple and easy way to reduce retrieval times. It is more useful for palm-print recognition if we can rank the candidate samples in the database

in descending order according to the aforementioned global features. Searching for the closest matches to a given query vector in a large database is time consuming if the vector is even moderately high dimensional. Various methods have been proposed to speed up the nearest neighbor retrieval, including hashing and tree structures [22]. However, the complexity of these methods grows exponentially with increasing dimensionality [23]. Therefore, we have adopted the RSVM method [20], inspired by the approaches of Internet search engines, to rank the candidate samples in the database.

Given a query q_k, $k = 1, 2, \ldots, n$ and a sample collection $D = \{d_1, d_2, \ldots, d_m\}$, the optimal retrieval system should return a ranking r_k^*, $k = 1, 2, \ldots, n$, that orders the samples in D according to their relevance to the query. In this paper, the query q and the sample d are the Γ-dimensional global features as described earlier. In our approach, if a sample d_i is ranked higher than d_j in some ordering r, i.e., $r(d_i) > r(d_j)$, then $(d_i, d_j) \in r$; otherwise, $(d_i, d_j) \notin r$. Consider the class of linear ranking functions

$$(d_i, d_j) \in f_{\vec{w}}(q) \Leftrightarrow \vec{w}\phi(q, d_i) > \vec{w}\phi(q, d_j) \tag{18}$$

where $\vec{w}$ is a weighted vector that is adjusted by learning and $\phi(q, d)$ is a pairwise distance function describing the match between q and d and can be defined as $\phi_i(q, d) = |q_i - d_i|$, $i = 1, \ldots, \Gamma$. Our goal is to find the optimal ranking function that will satisfy the maximum number of the following inequalities:

$$\begin{aligned} &\forall (d_i, d_j) \in r_1^* : \vec{w}\phi(q_1, d_i) > \vec{w}\phi(q_1, d_j) \\ &\qquad \cdots \\ &\forall (d_i, d_j) \in r_n^* : \vec{w}\phi(q_n, d_i) > \vec{w}\phi(q_n, d_j). \end{aligned} \tag{19}$$

It is easier to solve this problem if it is converted into the following SVM classification problem by introducing nonnegative slack variable $\xi_{i,j,k}$.

Hence, the problem is to minimize

$$V(\vec{w}, \vec{\xi}) = \frac{1}{2}\vec{w} \cdot \vec{w} + C \sum \xi_{i,j,k} \tag{20}$$

subject to

$$\begin{aligned} &\forall (d_i, d_j) \in r_1^* : \vec{w}\,(\phi(q_1, d_i) > \phi(q_1, d_j)) \geq 1 - \xi_{i,j,1} \\ &\qquad \cdots \\ &\forall (d_i, d_j) \in r_n^* : \vec{w}\,(\phi(q_n, d_i) > \phi(q_n, d_j)) \geq 1 - \xi_{i,j,n} \end{aligned} \tag{21}$$

$$\forall_i \forall_j \forall_k : \xi_{i,j,k} \geq 0 \tag{22}$$

where C is a parameter that allows trading off margin size against training error and $C = 0.1$ set by experience.

In the training stage, it is the inner-class samples of a test sample that should be ranked higher than the interclass samples, e.g., the inner-class samples' rank is one, and the interclass samples' rank is zero. We input the ranks together with the Γ-dimensional global features into the RSVM algorithm to learn the optimal ranking function $f_{\vec{w}^*}$. Given a new query q, the samples in the database can be sorted by their value of

$$rsv(q, d_i) = \vec{w}^* \phi(q, d_i). \tag{23}$$

TABLE I
EER OF 3-D PALM-PRINT VERIFICATION FOR $N = 4$, 8, AND 16 AND $M = 8$, 16, 32, AND 64 BY $MD + HCA + RLL$

	$M = 8$ EER (%)	$M = 16$ EER (%)	$M = 32$ EER (%)	$M = 64$ EER (%)
$N = 4$	14.30	19.15	14.35	14.07
$N = 8$	14.20	16.30	12.32	12.54
$N = 16$	18.11	18.35	15.21	14.11

TABLE II
EER OF 3-D PALM-PRINT VERIFICATION FOR $N = 8$ AND $M = 32$ BY MD, HCA, RLL, AND THEIR COMBINED RESULT

Global features	MD	HCA	RLL	MD+HCA+RLL
EER (%)	25.8	20.4	18.6	12.32

TABLE III
THREE-DIMENSIONAL PALM-PRINT RECOGNITION RATE BY OLDA FOR DIFFERENT DIMENSIONS

Γ	1	2	3	4	5	6	7
Recognition rate (%)	2	9.6	26	42.6	56.6	66.2	74.6
Γ	8	9	10	12	15	20	30
Recognition rate (%)	78.4	82.4	83.8	86	89.6	90.4	93.6

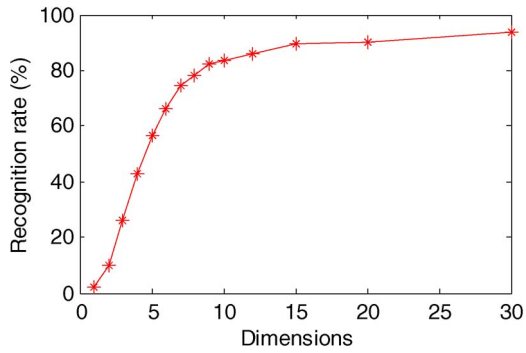

Fig. 10. Plot of 3-D palm-print recognition rate by OLDA for different dimensions.

IV. EXPERIMENTAL RESULTS

We used the 3-D palm-print acquisition device developed in [14] to establish a 3-D palm-print database containing 8000 samples collected from 400 palms. The 3-D palm-print samples were collected in two separated sessions, ten samples in each session. The average time interval between the two sessions is 1 month. The collection procedure required volunteers to put their palms naturally and without force on the device. The original spatial resolution of the data was 768 × 576. After ROI extraction, the central part (400 × 400) was extracted and downsampled to 200 × 200 for feature extraction and recognition.

The database was divided into a training part (the first session of 4000 samples) and a testing part (the second session of 4000 samples). As described in Section III, the dimension of the proposed global features is $1 + N + N \times M$. To select the values of M and N, we carried out a series of verifications on the training database where the class of the input palm print was known. Each of the 3-D samples was matched with the remaining samples in the training database. A successful match is where the two samples are from the same class. This is

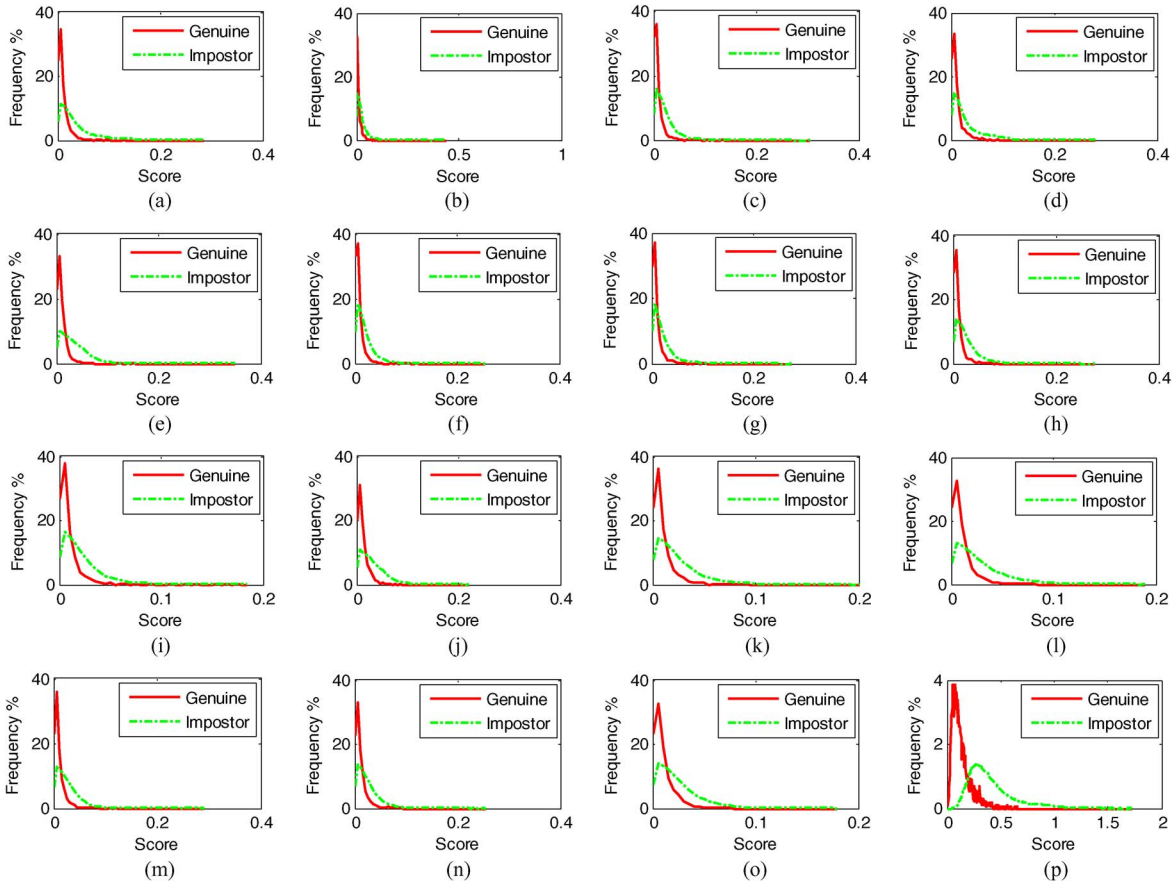

Fig. 11. Genuine and impostor distributions by the 3-D palm-print 15-dimensional global features. (a)–(o) are obtained by matching the single-dimension value from the 1st to 15th, and (p) is obtained by matching all 15-dimensional values together.

referred to as intraclass matching, and the candidate image is said to be genuine. An unsuccessful match is referred to as interclass matching, and the candidate image is said to be an impostor. Treating the global features as a point in the $1 + N + N \times M$ dimension space, we simply use the Euclidian distance as the matching score. Table I shows the equal error rate (EER) for $N = 4,\ 8,$ and 16 and $M = 8,\ 16,\ 32,$ and 64. The best result is $N = 8$ and $M = 32$.

In order to balance accuracy and efficiency, we chose $N = 8$ and $M = 32$ in the following experiments. This means that the global features have $1 + N + N \times M = 265$ dimensions. Table II shows the verification results by MD, HCA, RLL, and their combined results. From the last column of Table II, we can see that using the combined three global features will achieve a lower EER than using each of the individual features. As described in Section III-A, we use the OLDA method to reduce global features to a lower Γ dimension. To decide the optimal value of Γ, we carried out a series of recognition experiments on the 4000 sample training database. We divided this database into two equal parts, then chose the first five samples of every palm for training, and set aside the rest for testing. As shown in Section III-A, Γ is equal to q in (13). Instead of $q = rank(B)$, we let $q = 1, 2, \ldots, 10, 12, 15, 20, 30$. Table III and Fig. 10 show the recognition results. We can see that 15 dimensions are a good choice for the following coarse-level matching and RSVM schemes.

Fig. 11 shows the genuine and impostor distributions when the 3-D palm-print 15-dimensional global features are applied to the 4000 samples in the training database. Fig. 11(a)–(o) is obtained by using the Euclidian distance to match the single-dimension value from the 1st to 15th. Fig. 11(p) shows the result of using the Euclidian distance to match all 15-dimensional values.

We next carried out the 3-D palm-print classification and recognition experiments using the first sample of each class in the training database as a template and the 4000 samples in the testing database as probes, making a total of 400 templates and 4000 probes. The performance of classification and recognition is usually measured by error rate and penetration rate calculated in [21] as follows:

$$\text{error rate} = \frac{\text{number of false match}}{\text{total number of probe}} \times 100\% \tag{24}$$

$$\text{penetration rate} = \frac{\text{number of accessed templates}}{\text{total number of templates in the database}} \times 100\%. \tag{25}$$

Obviously, there is a tradeoff between error rates and penetration rates. Generally speaking, if there is no classification, there are two retrieval strategies: 1) all of the templates in

TABLE IV
PERFORMANCE COMPARISON OF THE THREE 3-D PALM-PRINT RECOGNITION APPROACHES

No classification		Coarse-level matching		RSVM	
Penetration rate (%)	Error rate (%)	Penetration rate (%)	Error rate (%)	Penetration rate (%)	Error rate (%)
100*	1.29	45.2	1.31	30	1.30
51.1	1.68	41.6	1.32	27.5	1.33
49.3	1.86	38.8	1.36	25	1.37
47.2	2.10	34.7	1.42	22.5	1.42
45.9	2.33	29.1	1.56	20	1.49
43.7	2.60	23.5	1.78	17.5	1.63
42.6	2.95	20.5	2.12	15	1.87
41.5	3.30	18.4	2.39	12.5	2.48
40.3	3.75	13.3	3.16	10	3.35
38.1	4.80	10.1	4.30	7.5	4.41
35.9	5.86	8.6	5.79	5	5.88

* This row used retrieval strategies 1) and the remaining rows used retrieval strategies 2) for no classification.

TABLE V
RUNNING TIME COMPARISON OF THE THREE 3-D PALM-PRINT RECOGNITION APPROACHES

	Once feature extraction time	Once dimensionality reduction time	Ranking or coarse matching time for all templates in database	Once matching time by MCI	Total running time for one probe testing
No classification	112ms	0ms	0ms	0.86ms	112+0.86*400*1.0 = 456ms
Coarse-level matching	136ms	0.1ms	0.5ms	0.86ms	136+0.1+0.5+0.86*400*0.452 = 292.09ms
RSVM	136ms	0.1ms	1.56ms	0.86ms	136+0.1+1.56+0.86*400*0.30 =240.86ms

the database are visited, and the template that gives the best matching score is regarded as the matched template if the matching score is less than a given threshold Ψ_T, and 2) given a threshold Ψ_t, the search continues until a match is found that is below that threshold.

We used three 3-D palm-print recognition matching approaches: 1) no classification; 2) coarse-level matching; and 3) RSVM. For no classification, we matched using the local feature MCI as described in [14]. The process we used for coarse-level matching is shown in Fig. 9 and involves fine-level matching using the local feature MCI. A single instance of coarse-level matching requires only 1/36 000 of the time it takes to do fine-level matching (coarse-level matching only needs 15 operations, while fine-level matching must do $128 \times 128 \times (8 \times 4 + 1)$ operations, where 128×128 is the size of ROI and $(8 \times 4 + 1)$ is the shifting template times). For the aforementioned two approaches, the penetration rate and the error rate will vary with different thresholds Ψ_t. As for RSVM, we use the RSVM algorithm described in Section III-C to rank the templates in the database and then match the top ρ percent by local feature MCI with the best matching score regarded as the matched template if this score is less than a given constant threshold Ψ_T. We can see from (25) that the ρ is equal to the penetration rate. Given different thresholds Ψ_t and ρ, we carried out a series of 3-D palm-print recognition experiments. Tables IV and V and Fig. 12 show these experimental results. Even at an approximately EER, the proposed coarse-level matching and RSVM approaches get a much lower penetration rate than the no-classification approach. Obviously, RSVM has the best performance but requires an additional offline training process compared to coarse-level matching.

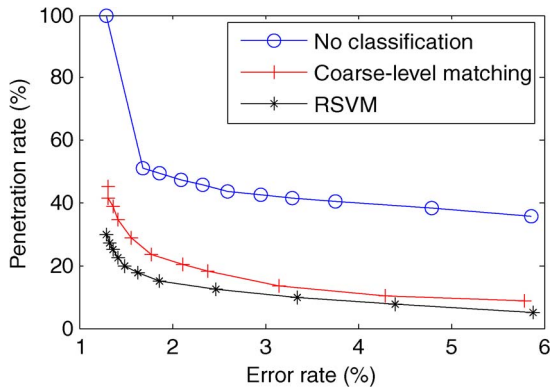

Fig. 12. Plot of the penetration rate and error rate of the three 3-D palm-print recognition approaches.

V. CONCLUSION

This paper has proposed three global features for 3-D palm-print images: MD, HCA, and RLL. These cannot be extracted from 2-D palm prints and are not correlated with local features, such as line and texture features. To make these global features efficient for use in coarse classification, we treat them as a multidimensional vector and use OLDA to map it to a lower dimensional space. We then improve the efficiency of 3-D palm-print recognition using two proposed approaches, coarse-level matching and RSVM, both of which significantly reduce the penetration rate during retrieval. Our recognition experiments using an established 3-D palm-print database of 8000 samples show that the global features improve palm-print classification which greatly reduces search times.

REFERENCES

[1] R. M. Bolle, J. H. Connell, S. Pankanti, N. K. Ratha, and A. W. Senior, *Guide to Biometrics*. New York: Springer-Verlag, 2003.

[2] A. W. K. Kong, D. Zhang, and G. M. Lu, "A study of identical twins' palmprints for personal verification," *Pattern Recognit.*, vol. 39, no. 11, pp. 2149–2156, Apr. 2006.

[3] A. K. Jain and J. J. Feng, "Latent palmprint matching," *IEEE Trans. Pattern Anal. Mach. Intell.*, vol. 31, no. 6, pp. 1032–1047, Jun. 2009.

[4] D. Zhang, A. W. K. Kong, J. You, and M. Wong, "On-line palmprint identification," *IEEE Trans. Pattern Anal. Mach. Intell.*, vol. 25, no. 9, pp. 1041–1050, Sep. 2003.

[5] A. W. K. Kong and D. Zhang, "Competitive coding scheme for palmprint verification," in *Proc. Int. Conf. Pattern Recogn.*, 2004, vol. 1, pp. 520–523.

[6] Z. N. Sun, T. N. Tan, Y. H. Wang, and S. Z. Li, "Ordinal palmprint representation for personal identification," in *Proc. IEEE Int. Conf. Comput. Vis. Pattern Recogn.*, 2005, pp. 279–284.

[7] X. Q. Wu, D. Zhang, and K. Q. Wang, "Palm line extraction and matching for personal authentication," *IEEE Trans. Syst., Man, Cybern. A, Syst., Humans*, vol. 36, no. 5, pp. 978–987, Sep. 2006.

[8] D. S. Huang, W. Jia, and D. Zhang, "Palmprint verification based on principal lines," *Pattern Recognit.*, vol. 41, no. 4, pp. 1316–1328, Apr. 2008.

[9] C. Samir, A. Srivastava, and M. Daoudi, "Three-dimensional face recognition using shapes of facial curves," *IEEE Trans. Pattern Anal. Mach. Intell.*, vol. 28, no. 11, pp. 1858–1863, Nov. 2006.

[10] G. Medioni, J. Choi, C. H. Kuo, and D. Fidaleo, "Identifying noncooperative subjects at a distance using face images and inferred three-dimensional face models," *IEEE Trans. Syst., Man, Cybern. A, Syst., Humans*, vol. 39, no. 1, pp. 12–24, Jan. 2009.

[11] P. Yan and K. W. Bowyer, "Biometric recognition using 3D ear shape," *IEEE Trans. Pattern Anal. Mach. Intell.*, vol. 29, no. 8, pp. 1297–1308, Aug. 2007.

[12] V. Srinivassan and H. C. Liu, "Automated phase measuring profilometry of 3D diffuse object," *Appl. Opt.*, vol. 23, no. 18, pp. 3105–3108, Sep. 1984.

[13] H. O. Saldner and J. M. Huntley, "Temporal phase unwrapping: Application to surface profiling of discontinuous objects," *Appl. Opt.*, vol. 36, no. 13, pp. 2770–2775, May 1997.

[14] D. Zhang, G. Lu, W. Li, L. Zhang, and N. Luo, "Palmprint recognition using 3-D information," *IEEE Trans. Syst., Man, Cybern. C, Appl. Rev.*, vol. 39, no. 5, pp. 505–519, Sep. 2009.

[15] W. Li, D. Zhang, G. M. Lu, and N. Luo, "A novel 3-D palmprint acquisition system," *IEEE Trans. Syst., Man, Cybern. A, Syst., Humans*, vol. 42, no. 2, pp. 443–452, Mar. 2012.

[16] E. Henry, *Classification and Uses of Fingerprints*. London, U.K.: Routledge, 1900.

[17] X. Q. Wu, D. Zhang, K. Q. Wang, and B. Huang, "Palmprint classification using principal lines," *Pattern Recognit.*, vol. 37, no. 10, pp. 1987–1998, 2004.

[18] A. Lumini, D. Maio, and D. Maltoni, "Continuous vs. exclusive classification for fingerprint retrieval," *Pattern Recognit. Lett.*, vol. 18, no. 10, pp. 1027–1034, Oct. 1997.

[19] J. P. Ye, "Characterization of a family of algorithms for generalized discriminant analysis on undersampled problems," *J. Mach. Learn. Res.*, vol. 6, pp. 483–502, Apr. 2005.

[20] T. Joachims, "Optimizing search engines using clickthrough data," in *Proc. 8th ACM SIGKDD*, 2002, pp. 133–142.

[21] D. Maltoni, D. Maio, A. K. Jain, and S. Prabhakar, *Handbook of Fingerprint Recognition*. New York: Springer-Verlag, 2003.

[22] B. Matei, Y. Shan, H. Sawhney, Y. Tan, R. Kumar, D. Huber, and M. Hebert, "Rapid object indexing using locality sensitive hashing and joint 3D signature space estimation," *IEEE Trans. Pattern Anal. Mach. Intell.*, vol. 28, no. 7, pp. 1111–1126, Jul. 2006.

[23] H. Chen and B. Bhanu, "Efficient recognition of highly similar 3D objects in range images," *IEEE Trans. Pattern Anal. Mach. Intell.*, vol. 31, no. 1, pp. 172–179, Jan. 2009.

Bob Zhang (M'12) received the M.A.Sc. degree in information systems security from Concordia University, Montreal, QC, Canada, in 2007 and the Ph.D. degree in electrical and computer engineering from the University of Waterloo (UW), Waterloo, ON, in 2011.

He is currently a Researcher with UW Center for Pattern Analysis and Machine Intelligence, Department of Electrical and Computer Engineering, UW. He is also with Biometrics Research Center, Department of Computing, The Hong Kong Polytechnic University, Kowloon, Hong Kong. His research interests include pattern recognition, machine learning, and medical biometrics.

Wei Li received the B.S. degree from Luoyang Institute of Technology, Luoyang, China, in 2001, the M.S. degree in mechanical and electrical engineering from Henan University of Science and Technology, Luoyang, in 2005, and the Ph.D. degree in pattern recognition and intelligent systems from Shanghai Jiao Tong University, Shanghai, China, in 2010.

He is an Assistant Researcher with Shenzhen Institutes of Advanced Technology, Chinese Academy of Sciences, Shenzhen, China. He is also with Huawei Technologies Company, Ltd., Shenzhen. His research interests include pattern recognition, image processing, graphics, cloud computing, and virtualization.

Pei Qing received the B.Eng. degree in computer science and technology from Tsinghua University, Beijing, China, in 2010. He is currently working toward the M.S. degree in software technology in the Department of Computing, The Hong Kong Polytechnic University, Kowloon, Hong Kong.

From 2010 to 2011, he was a Computer Graphics Developer with Virtuos Company Ltd., Shanghai, China. His current research interests include pattern recognition, image processing, and biometrics.

David Zhang (M'89–SM'95–F'08) received the B.S. degree in computer science from Peking University, Beijing, China, the M.Sc. degree in computer science and the Ph.D. degree from Harbin Institute of Technology (HIT), Harbin, China, in 1982 and 1985, respectively, and the second Ph.D. degree in electrical and computer engineering from the University of Waterloo, Waterloo, ON, Canada, in 1994.

From 1986 to 1988, he was a Postdoctoral Fellow with Tsinghua University, Beijing, and then an Associate Professor with the Academia Sinica, Beijing. He is currently a Chair Professor with The Hong Kong Polytechnic University, Kowloon, Hong Kong, where he is the Founding Director of the Biometrics Research Center (University Grants Committee/Collaborative Research Center) supported by the Hong Kong, Special Administrative Region, Government in 1998. He also serves as a Visiting Chair Professor with Tsinghua University and an Adjunct Professor with Peking University, Shanghai Jiao Tong University, Shanghai, China, HIT, and the University of Waterloo. He is the Founder and Editor-in-Chief of International Journal of Image and Graphics, Book Editor of Springer International Series on Biometrics (KISB), Organizer of the International Conference on Biometric Authentication, Associate Editor of more than ten international journals including IEEE Transactions and Pattern Recognition, and the author of more than ten books and 250 journal papers.

Dr. Zhang is a Croucher Senior Research Fellow, Distinguished Speaker of the IEEE Computer Society, and a fellow of International Association for Pattern Recognition.